A Lidar-Based Decision-Making Method for Road Boundary Detection Using Multiple Kalman Filters

Yeonsik Kang, Chiwon Roh, Seung-Beum Suh, and Bongsob Song

***Abstract*—In this paper, a novel decision-making method is proposed for autonomous mobile robot navigation in an urban area where global positioning system (GPS) measurements are unreliable. The proposed method uses lidar measurements of the road's surface to detect road boundaries. An interacting multiple model method is proposed to determine the existence of a curb based on a probability threshold and to accurately estimate the roadside curb position. The decision outcome is used to determine the source of references suitable for reliable and seamless navigation. The performance of the decision-making algorithm is verified through extensive experiments with a mobile robot autonomously navigating through campus roads with several intersections and unreliable GPS measurements. Our experimental results demonstrate the reliability and good tracking performance of the proposed algorithm for autonomous urban navigation.**

***Index Terms*—Curb detection, mobile robot control, outdoor navigation, road boundary detection.**

I. Introduction

THE availability of modern global positioning systems (GPSs) has allowed significant improvements in mobile robot navigation technologies in outdoor environments. Combined with complementary dead-reckoning sensors such as encoders, inertial measurement unit, and geomagnetic sensors, GPS measurements are used to update the global position estimate of a mobile robot without concern for the accumulation of errors. For example, extended Kalman filters are often used to integrate multiple sensor measurements and accurately estimate the position of the robot [1]–[4]. However, there is much concern about the reliability of outdoor localization in an urban environment, where GPS signals are often blocked by adjacent high-rise structures. In order to operate a fully automated patrol robot for security or autonomous transportation systems in such an environment, the use of environmental features that are extracted from sensor measurements such as lidar or camera vision is a good alternative, as described in [5]–[8].

Curb detection and tracking is one of the most efficient techniques for extracting environmental information in an urban environment [9]. The idea is to detect the boundaries of a paved road using lidar measurements and to control the robot to maintain a certain distance from the boundaries. Such a method has been popular among the researchers who develop the road boundary detection algorithms in [10]–[13], since most of the urban road boundaries are distinguishable by analyzing the lidar scan profile. In [10], an eigenvector technique was used to find a line segment corresponding to the edges of the road. In [11], a Hough transform was used to find the best fit line to the surface on the road. End points corresponding to the best fit line were used as the curb points of the road. In [13], a discrete wavelet transform is used to extract the curb points from the lidar data set.

Although researchers have proposed methods for road boundary detection and tracking, a detailed analysis of how to initiate or terminate tracking to systematically deal with a mobile robot that enters or leaves an intersection has not been carried out. When the mobile robot enters an intersection, the robot should discontinue its control mode of curb following and switch to dead-reckoning mode until it passes the intersection. In such a situation, the mobile robot should be able to distinguish whether there is a curb in its sensor field of view and determine the moment when it is best to switch its control mode. This decision is very critical for reliable navigation because the robot may move in the wrong direction if it switches to dead reckoning too late, or it may not be able to follow the curb after it passes the intersection. Robustness between changes in the control mode is very important in order to achieve reliable and seamless navigation.

In this paper, a decision-making method is proposed for the robust urban navigation of autonomous mobile robots. A measurement model is developed to describe the noise characteristics of roadside curb point features using lidar sensors. The developed model is used during the update process for the two Kalman filters; each is based on a different hypothesis regarding the existence of the curb. The method of using a multiple Kalman-filter bank originates from the probabilistic interacting multiple model (IMM) method. IMM is a probabilistic approach since its decision criterion is based on the threshold of model probability which describes how much the model can be trusted. IMM was originally developed in the aerospace industry for the accurate tracking of multiple targets

Manuscript received December 28, 2010; revised May 17, 2011 and August 31, 2011; accepted November 30, 2011. Date of publication January 18, 2012; date of current version June 19, 2012. This work was supported in part by the Basic Science Research Program through the National Research Foundation of Korea funded by the Ministry of Education, Science and Technology under Grant 2011-0013500 and in part by the Faculty Research Program 2011 of Kookmin University in Korea.

Y. Kang is with the Department of Automotive Engineering, Kookmin University, Seoul 136-702, Korea (e-mail: yeonsikkang@gmail.com).

C. Roh is with the Yujin Robot Company, Ltd., Seoul 153-802, Korea (e-mail: chiwon.roh@gmail.com).

S.-B. Suh is with the Korea Institute of Science and Technology, Seoul 136-791, Korea (e-mail: keenhurt@kist.re.kr).

B. Song is with the Department of Mechanical Engineering, Ajou University, Suwon 443-749, Korea (e-mail: bsong@ajou.ac.kr).

Color versions of one or more of the figures in this paper are available online at http://ieeexplore.ieee.org.

Digital Object Identifier 10.1109/TIE.2012.2185013

detected by radar measurements. The method has been used in many different applications such as detecting the maneuvers of other vehicles on the road [14]–[16]. Many studies (e.g., [17]–[19]) have used IMM for the detection and diagnosis of actuator and sensor faults. The method is numerically efficient compared to the multiple hypothesis test detector and is superior to many other multiple model-based approaches such as multiple model adaptive estimation and its variants. The IMM algorithm used in this study provides a real-time solution to enable a robot to react to environmental changes.

The IMM method has been employed for accurate tracking of the curb position in the literature such as [10] and [12]. However, in this study, IMM is used for decision making regarding the existence of the curb in order to improve the reliability of autonomous navigation, particularly when the robot is passing intersections. This decision may also be made by checking the geometric profile of a lidar scan of the road's surface. However, an incorrect switch of the control mode may cause a significant failure in the operation of autonomous navigation. Therefore, the best strategy is to include as much evidence as possible to choose the time at which the control mode is changed. Combined with other clues such as the geometric features of the road scan profile or GPS measurements of the mobile robot, the proposed method decreases the rate of false decision and enhances seamless navigation in an urban environment with intersections.

The remainder of this paper is organized as follows. In Section II, the curb measurement and prediction model will be presented based on the geometrical relationship between the mobile robot and the curb. In Section III, a probabilistic decision-making strategy will be explained in detail with a brief explanation of the general IMM algorithm. Experimental results will be presented in Section IV followed by the conclusion in Section V.

II. Curb Prediction and Measurement Models

A. Curb Detection Method

Lidar has become one of the most popular sensors used in mobile robot navigation due to its accuracy and robustness in outdoor environments. In this paper, we used lidar to provide road surface and boundary information. A lidar sensor is mounted on the mobile robot as shown in Fig. 1, with its scanning plane tilted by as much as α below the horizontal plane. Since the curb height is uniform in most urban areas, a tilted scanning plane provides a uniform geometrical feature as shown by the dotted line in Fig. 1. The lidar measurements (ξ_i, η_i), $i \in (1, 2, \ldots, m)$, are defined in the tilted scanning plane in coordinates defined by X_v and Y_v^t, whereas the curb position (x_c, y_c) is defined using X_v and Y_v coordinates.

In this paper, a Hough transform-based method is used to detect the curb point (x_c, y_c) using geometrical features. By applying the Hough transform to the lidar scan, a line equation that best represents the road surface, $\gamma = \xi\cos(\sigma) + \eta\sin(\sigma)$, is determined where σ and γ represent the angle and length of the normal vector drawn from the origin to the line, respectively. Second, a set of lidar measurements (ξ_i, η_i) is found that

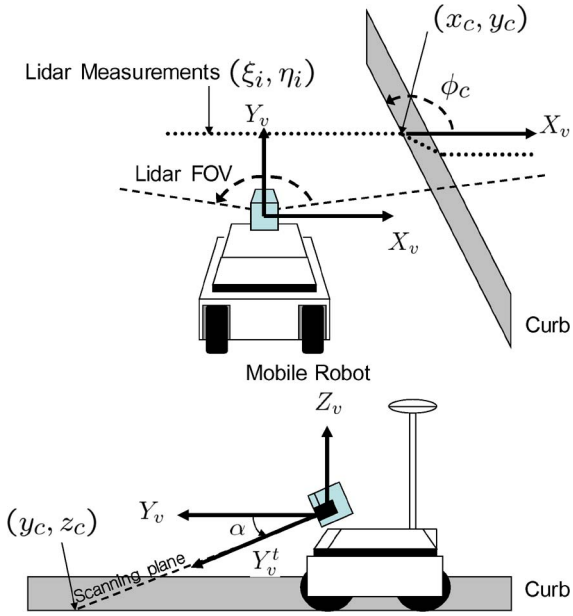

Fig. 1. Curb position described by a lidar-fixed coordinate system.

were within a δ distance from the line equation in a horizontal plane

$$|\xi_i\cos(\sigma) + \eta_i\sin(\sigma) + \gamma| < \frac{\delta}{\cos(\alpha)} \tag{1}$$

where α represents the tilted angle of the lidar with respect to the horizontal plane. Finally, the road edge point is estimated by finding the last measurement (ξ_c, η_c) in the set of lidar measurements that satisfies the distance and angle conditions (2) and (3) and projecting this measurement to the horizontal plane of X_v and Y_v coordinates

$$\sqrt{(\xi_i - \xi_{i+1})^2 + (\eta_i - \eta_{i+1})^2} \le \rho_d \tag{2}$$

$$\left|\tan^{-1}\left(\frac{\eta_i - \eta_{i+1}}{\xi_i - \xi_{i+1}}\right)\right| \le \kappa_d \tag{3}$$

where ρ_d and κ_d represent the thresholds regarding the distance and angle between the two consecutive lidar measurements, respectively. The details of the employed curb detection method are illustrated in [11].

In Fig. 2, the dotted line represents the lidar measurements (ξ_i, η_i) projected to X_v and Y_v coordinates, and the circle represents the results of the curb detection method using the aforementioned conditions described by (1)–(3). In Fig. 2(a), a curb exists about 1 m from the robot since the robot is controlled to keep 1-m distance from the curb. In Fig. 2(b), the curb disappears on the right side of the robot, and the elevated profile of the intersection is measured by the lidar scan. Although the curb disappears, the curb detection algorithm still outputs the outermost points within a predetermined threshold δ which is set to 15 cm in this case. This example illustrates the need for an intelligent algorithm to determine the existence of the curb based on more evidences than the geometric shape alone.

The projection of the feature measurement (ξ_c, η_c) yields the measurement vector (z_x, z_y) for the estimation of the curb

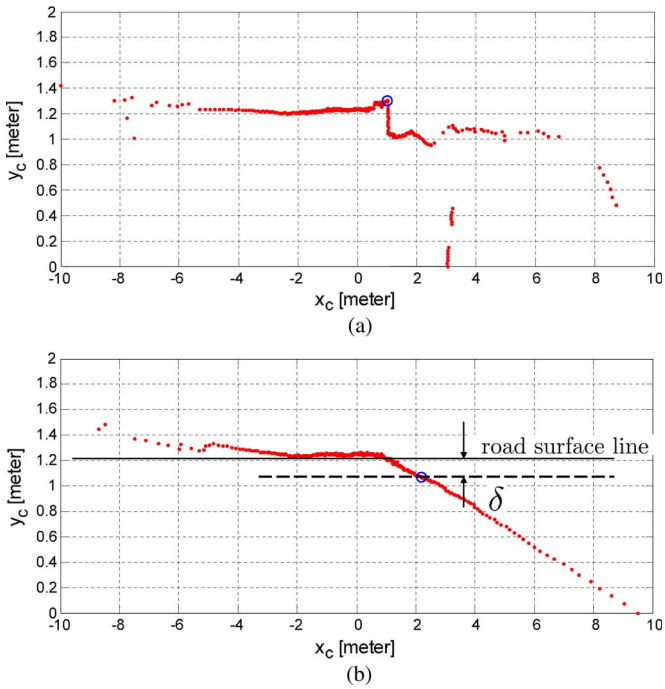

Fig. 2. (a) (Blue circle) Correct position of curb measured by the curb detection algorithm when a curb is present. (b) Example of incorrect curb detection when a curb is not present in the lidar sensor field of view.

point (x_c, y_c). In addition, the relative orientation measurement z_ϕ is obtained approximately by finding a linear least squares estimate that approximates a curb surface next to the curb point of (ξ_c, η_c). Assuming a uniform curb height, the number of lidar measurements corresponding to the curb face can be calculated by using tilting angle α and the curb height.

B. Curb Measurement Model

The measurement model of the curb position (x_c, y_c) and the relative angle ϕ_c, between the road tangent line of the curb and the X_v^k coordinates, is used for the update process of the Kalman filter. z_c is not of interest in this study because its value remains constant for a flat road surface.

Fig. 3 shows that the lidar scans the surface of the road with an angular resolution of $\Delta\theta$. Since lidar provides a very accurate range measurement in general, the angular resolution of the scanning beam is the major source of uncertainty in the curb position measurement. A fixed lidar tilting angle α provides a constant scanning distance $\bar{y} = \sqrt{y_c^2 + z_c^2}$, under the assumption of a flat road surface. Hence, y_c is regarded as a nearly constant value. The uncertainty caused by the finite beam resolution affects the measurement model of x_c.

The curb point measurement of (x_c, y_c) is denoted by (z_x, z_y). Then, x_c exists between $(z_x, z_x + \Delta_c)$ because the finite resolution of the beam $\Delta\theta$ determines the quantization error Δ_c. X_v^k and Y_v^k represent the robot-fixed coordinate system at k. The relation between Δ_c and z_x is determined by the geometrical relation that is defined as follows:

$$z_x + \Delta_c = \bar{y}\tan(\theta + \Delta\theta). \tag{4}$$

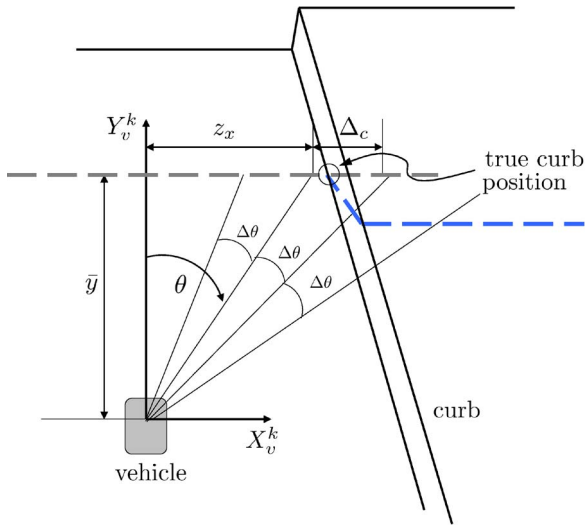

Fig. 3. Quantization error Δ_c of curb position measurement with respect to the lidar beam resolution $\Delta\theta$.

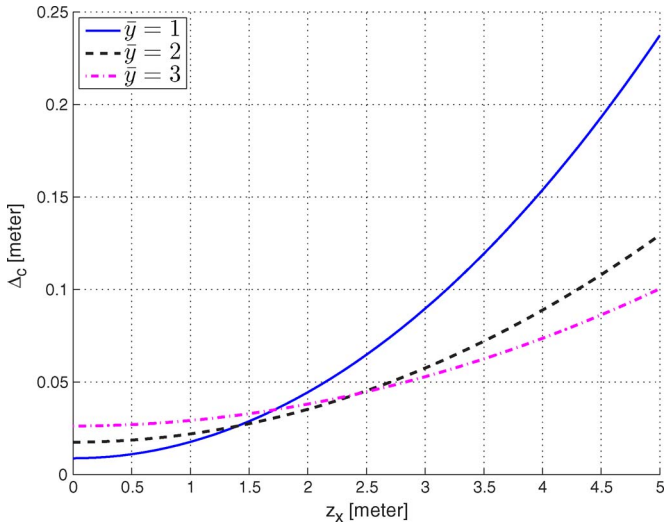

Fig. 4. Quantization error growth of curb position measurement with respect to z_x caused by lidar beam resolution.

Using the relation $\tan(A + B) = (\tan A + \tan B)/(1 - \tan A \tan B)$, Δ_c can be determined by

$$\Delta_c = \frac{(z_x^2 + \bar{y}^2)}{\bar{y} - z_x \tan\Delta\theta} \tan\Delta\theta. \tag{5}$$

Fig. 4 shows how Δ_c grows with respect to z_x, which increases faster than a quadratic function of z_x. If $\bar{y} = 2$, the error increases from 0.02 to 0.135 m as z_x increases from 1 to 5 m. Assuming that the probability distribution of the curb position x_c is uniform between z_x and $z_x + \Delta_c$, the probability density function $p_{x_c}(x)$ and the variance of x_c are defined as

$$p_{x_c}(x) = \begin{cases} \frac{1}{\Delta_c} & \text{if } z_x \le x \le z_x + \Delta_c \\ 0 & \text{otherwise} \end{cases} \tag{6}$$

$$\text{mean}(x_c) = z_x + \frac{\Delta_c}{2} \quad \text{var}(x_c) = \frac{\Delta_c^2}{12}. \tag{7}$$

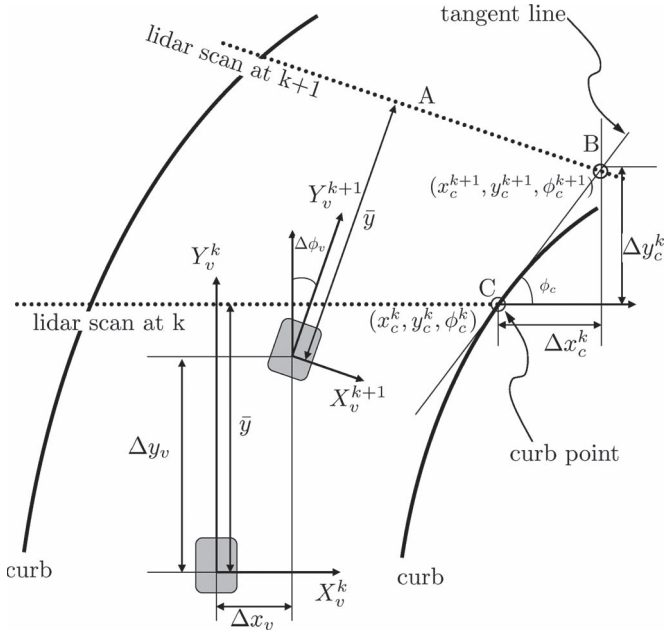

Fig. 5. Coordinate system and the geometry of the curb position relative to the mobile robot.

In this paper, the uniform quantization error distribution is approximated using a Gaussian probability distribution with zero mean and variance as given by (7).

Hence, the measurement equations for (z_x, z_y, z_ϕ) are represented by

$$\begin{aligned} z_x(k) + \frac{\Delta_c}{2} &= x_c(k) + w_x(k) \\ z_y(k) &= y_c(k) + w_y(k) \\ z_\phi(k) &= \phi_c(k) + w_\phi(k) \end{aligned} \tag{8}$$

where $w_x(k)$, $w_y(k)$, and $w_\phi(k)$ are the measurement noises for individual measurements z_x, z_y, and z_ϕ, respectively. Finally, the measurement model is summarized by

$$\mathbf{z}(k) = \mathbf{H}\mathbf{x}(k) + \mathbf{w}(k) \tag{9}$$

where $\mathbf{z}(k) = [z_x(k) + \Delta_c/2, z_y(k), z_\phi(k)]^T$ represents the measurement vector, $\mathbf{H}$ is the 3×3 identity matrix, $\mathbf{x}(k) = [x_c(k), y_c(k), \phi_c(k)]^T$ represents the state vector of the curb point, and $\mathbf{w}(\mathbf{k})$ is assumed to be Gaussian measurement noise with covariance matrix $\mathbf{E}[\mathbf{w}(k)\mathbf{w}(k)^T] = \mathbf{R}$.

C. Curb Prediction Model

In Fig. 5, the coordinate system and the geometry of the relative curb position with respect to the mobile robot are shown following the approach presented in [10].

The intersection point between the scanning plane and the curb is defined by (x_c^k, y_c^k, ϕ_c^k) in the X_v^k, Y_v^k coordinate system. ϕ_c^k represents the angle between the tangent line of the curb and the X_v^k axis. The superscript k denotes the corresponding coordinate system, whereas (k) represents the parameter at time k. If the road is straight, a new intersection point $(x_c^{k+1}, y_c^{k+1}, \phi_c^{k+1})$ can be found on the tangent line of the previous intersection point as the vehicle moves by Δx_v^k and Δy_v^k along the X_v^k and Y_v^k axes, respectively, and changes its direction of heading by $\Delta\phi_v^k$ in the counterclockwise direction. Based on this straight-road assumption, the discrete-time dynamic equations are modeled by

$$\mathbf{x}^{k+1}(k+1) = f\left(\mathbf{x}^k(k), \mathbf{u}(k)\right) + \mathbf{v}(k) \tag{10}$$

where

$$\begin{aligned} &\mathbf{x}^k(k) \\ &\quad = \left[x_c^k(k), y_c^k(k), \phi_c^k(k)\right]^T \\ &f\left(\mathbf{x}^k(k), \mathbf{u}(k)\right) \\ &\quad = \mathbf{F}(\mathbf{k})\mathbf{x}^k(k) + \mathbf{u}(k) \\ &\mathbf{F}(k) \\ &\quad = \begin{bmatrix} \cos\left(\Delta\phi_v^k\right) & \sin\left(\Delta\phi_v^k\right) & 0 \\ -\sin\left(\Delta\phi_v^k\right) & \cos\left(\Delta\phi_v^k\right) & 0 \\ 0 & 0 & 1 \end{bmatrix} \\ &\mathbf{u}(k) \\ &\quad = \begin{bmatrix} \left(\Delta x_c^k - \Delta x_v^k\right)\cos\Delta\phi_v^k + \left(\Delta y_c^k - \Delta y_v^k\right)\sin\Delta\phi_v^k \\ -\left(\Delta x_c^k - \Delta x_v^k\right)\sin\Delta\phi_v^k + \left(\Delta y_c^k - \Delta y_v^k\right)\cos\Delta\phi_v^k \\ \Delta\phi_v^k \end{bmatrix}. \end{aligned}$$

Because the discrete dynamics are the same for both the left- and right-side curb points, only the right-side curb is shown in Fig. 5. Note that $\mathbf{v}(k)$ is assumed to be Gaussian process noise with covariance matrix $Q(k)$. The input variables for $\mathbf{u}(k)$ are determined by the following geometrical relations:

$$\begin{aligned} \Delta x_c^k &= \frac{c_{BC} - c_{AB}}{m_{AB} - m_{BC}} - z_x^k - \frac{\Delta_c}{2} \\ \Delta y_c^k &= m_{AB}\frac{c_{BC} - c_{AB}}{m_{AB} - m_{BC}} + c_{AB} - z_y^k \\ m_{AB} &= \tan\left(\Delta\phi_v^k\right) \\ c_{AB} &= \Delta y_v^k + \bar{y}\cos\Delta\phi_v^k - \tan\Delta\phi_v^k\left(\Delta x_v^k - \sin\Delta\phi_v^k\right) \\ m_{BC} &= \tan z_\phi^k \\ c_{BC} &= z_y^k - m_{BC} z_x^k \\ \Delta x_v^k &= -V\Delta T\sin\Delta\phi_v^k \\ \Delta y_v^k &= V\Delta T\cos\Delta\phi_v^k. \end{aligned}$$

In the aforementioned equations, m_{ij} and c_{ij} represent the slope and the intercept of the line passing through the points i and j, respectively, when the line is defined by $y_v^k = m_{ij}x_v^k + c_{ij}$. It is assumed that the change of heading $\Delta\phi_v^k$ and the robot's velocity V can be measured by the sensor such as wheel speed or yaw rate sensor. (z_x^k, z_y^k, z_ϕ^k) represents the measurement data defined in Section II-B at time k.

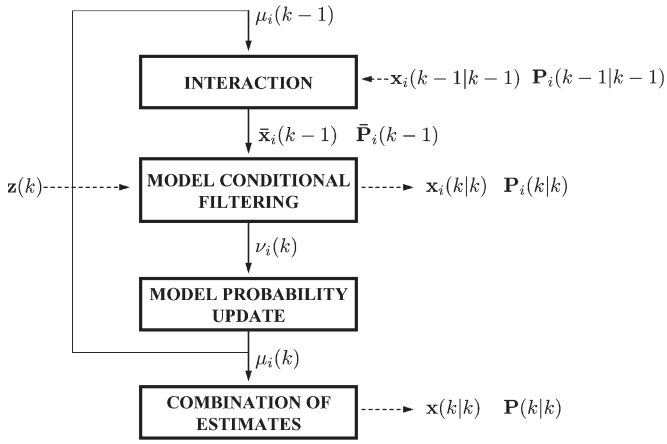

Fig. 6. Four major steps of a general IMM algorithm.

III. Decision Making Using IMM

Thus far, this paper has described a method of using Kalman filters to accurately track intersection points between a lidar-scanned surface and a curb. However, when the mobile robot follows the road, the existence of a curb becomes very important information that determines the best control strategy for the reliable navigation. In this section, a method is proposed to determine the existence of a curb in the sensor's field of view using procedures based on the IMM method.

A. IMM Method

The IMM algorithm is a hybrid estimator that contains both finite and continuous states to model the dynamics of a system. Therefore, the IMM estimator runs a finite number of Kalman filters based on different models. The state transitions between finite models are assumed to follow a Markov model. The model probability is calculated to provide an indication of the particular state in effect at each time. Finally, probabilistic decision making is allowed based on the model probability at the moment [17].

The general IMM algorithm consists of four major steps as shown in Fig. 6.

In the "model conditional filtering" step, sensor measurements are fed to the model conditional filter bank that contains N Kalman filters, each based on a different model. Each Kalman filter calculates the state estimates $\mathbf{x}_i(k|k)$, covariances $\mathbf{P}_i(k|k)$, and residuals $\nu_i(k)$ with $i \in \{0, 1, 2, \cdots, N-1\}$. Next, in the "model probability update" step, the model probability $\mu_i(k)$ is calculated depending on the measurement residual $\nu_i(k)$ using a predefined likelihood function for each model. The likelihood function is defined using the measurement models derived in Section II-A. In the "combination of estimates" step, the model probability is used to calculate the final estimates $\mathbf{x}(k|k)$ with covariance $\mathbf{P}(k|k)$. The kth iteration is complete after the "combination of estimates" step. At the next $k+1$th "interaction" step, the initial state of the model conditional filter $\bar{x}_i(k)$ is recalculated using the Markov model transition probability and the previous filter estimates $\mathbf{x}_i(k)$. The details of the IMM algorithm are given in [20]–[23].

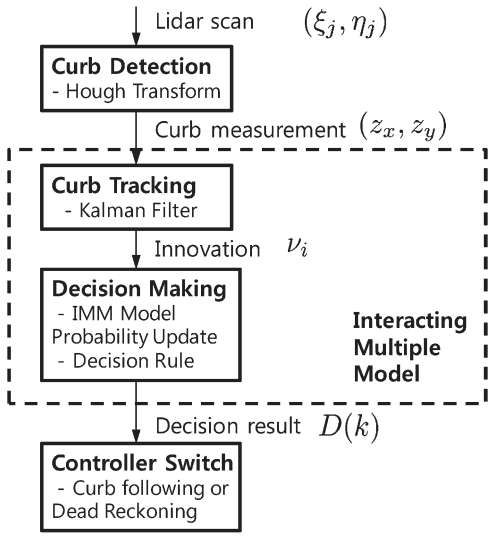

Fig. 7. Schematic of process to make a decision regarding curb existence using the IMM algorithm.

B. Probabilistic Decision Making

Fig. 7 shows the overall layout of the decision-making and curb-tracking processes proposed in this study. The first two steps, "curb detection" and "curb tracking," are described in Section II.

The "curb detection" step yields the curb position measurements by extracting a feature point in the lidar scan profile. In the "curb tracking" step, two Kalman filters are run using the same prediction model but with different measurement models. One is based on the model $i = 1$, with the assumption that the curb point measurement is true. The other is based on the model $i = 0$, with the assumption that the curb point measurement is false or that the curb does not exist in the lidar's field of view. Based on these two assumptions, the likelihood functions of the measurement residual are determined by

$$\Lambda_i(k) = \mathcal{N}\{\nu_i(k); 0, S_i(k)\} \tag{11}$$

which assumes a Gaussian distribution of the residual $\nu_i(k)$. $S_i(k)$ represents the measurement error covariance matrix of the corresponding model. Although the model with $i = 0$ assumes that the curb does not exist in the lidar's field of view, the curb detection algorithm explained in Section II-A outputs irregular false detection results as shown in Fig. 2(b). Therefore, this model features greater measurement noise covariance than the model with $i = 1$.

The "decision making" step uses the likelihood function defined by (11) to update the model probability as follows:

$$\mu_i(k) = \frac{\Lambda_i(k)\bar{\mu}_i(k)}{\sum_{j=0}^{1} \Lambda_j(k)\bar{\mu}_j(k)} \tag{12}$$

where $\bar{\mu}_i(k)$ is calculated at the previous interaction step by

$$\bar{\mu}_i(k) = \sum_{j=0}^{1} \pi_{ji}\mu_j(k-1). \tag{13}$$

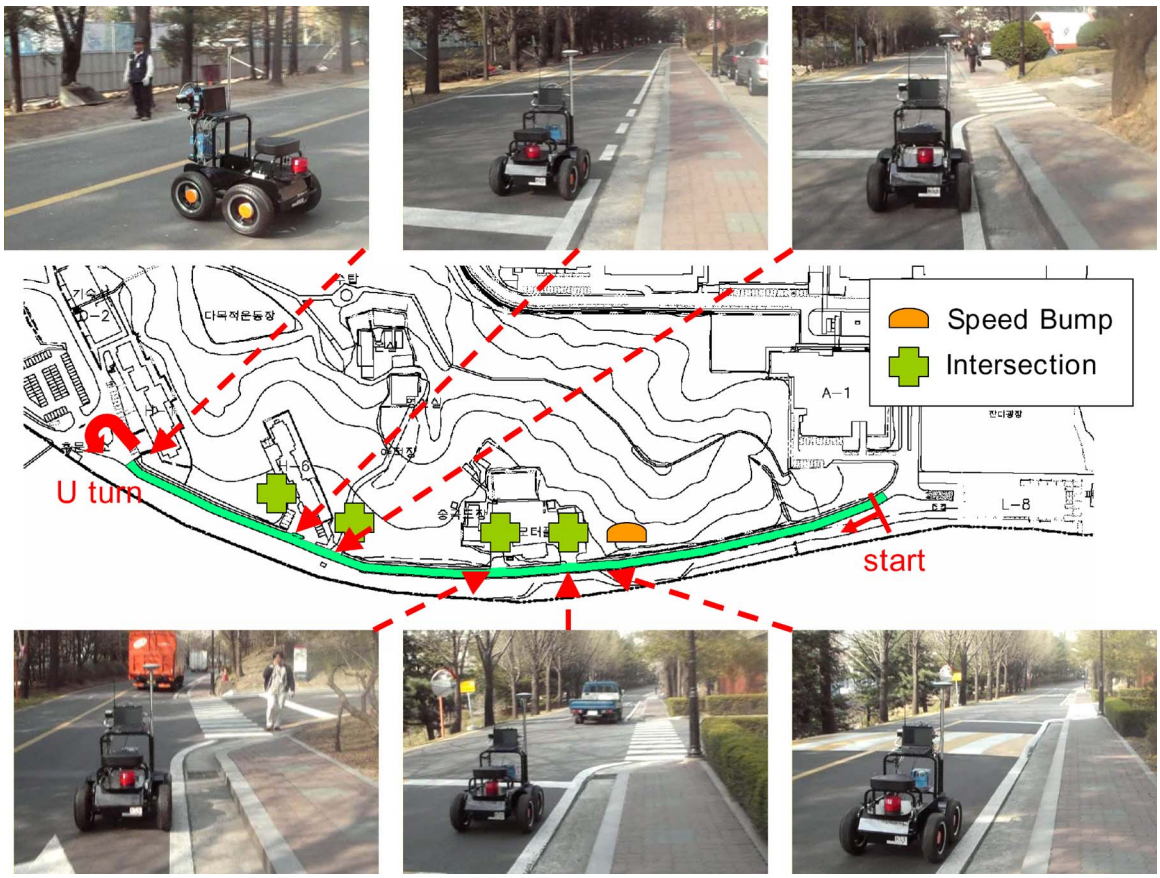

Fig. 8. Map of the experimental site. Pictures show the mobile robot at the intersections, speed bump, and return point.

In (13), π_{ij} represents the Markov transition probability matrix. Finally, the decision rule for the existence of the curb is defined by

$$D(k)=0 \text{ if } \begin{cases} D(k-1)=0, & \mu_1(k)<\mu_{\text{high}} \\ D(k-1)=1, & \mu_1(k)<\mu_{\text{low}} \end{cases}$$
$$D(k)=1 \text{ if } \begin{cases} D(k-1)=0, & \mu_1(k)>\mu_{\text{high}} \\ D(k-1)=1, & \mu_1(k)>\mu_{\text{low}} \end{cases} \quad (14)$$

where $\mu_{\text{high}} > \mu_{\text{low}}$ and $D(k)$ is a decision variable that switches between one and zero. The decision rule works as a flag that switches when a threshold condition for $\mu_1(k)$ is satisfied. The decision rule enables the current navigation control strategy to switch between the "curb-following mode" when $D(k)=1$ and the "intersection-crossing mode" when $D(k)=0$.

TABLE I
PARAMETERS FOR IMM ALGORITHM

IMM Parameters	Values
π_{ij}	$\begin{bmatrix} 0.001 & 0.999 \\ 0.01 & 0.99 \end{bmatrix}$
μ_{high}	0.9
μ_{low}	0.1
S_0	$\begin{bmatrix} 3\Delta_c^2 & 0. & 0. \\ 0. & 0.02 & 0. \\ 0. & 0. & 0.24 \end{bmatrix}$
S_1	$\begin{bmatrix} \frac{\Delta_c^2}{12} & 0. & 0. \\ 0. & 0.02 & 0. \\ 0. & 0. & 0.04 \end{bmatrix}$

IV. EXPERIMENTAL RESULTS

Two types of control mode were implemented in the control software architecture of the experimental hardware platform: the curb-following control mode and the intersection-crossing mode. Along a curbed road, the mobile robot follows the curb approximately 1 m away using the curb-following controller. However, when the robot passes an intersection, it relies on its dead-reckoning ability to maintain the desired direction. The switching of the control mode is based on the decision rule given by (14). The controller design for the curb-following and dead-reckoning modes is based on [24] and [25], respectively.

The experimental platform is a four-wheeled skid-type mobile robot equipped with lidar, an inertial measurement unit, a GPS, an attitude sensor, encoders, and camera vision. Fig. 8 shows a map of the route where the developed algorithm was experimented. On the route, there are four intersections where the curb is discontinued. The mobile robot follows the road keeping a distance of approximately 1 m from the curb to avoid blocking nearby traffic. The global position estimate is calculated based on the GPS and inertial measurements to

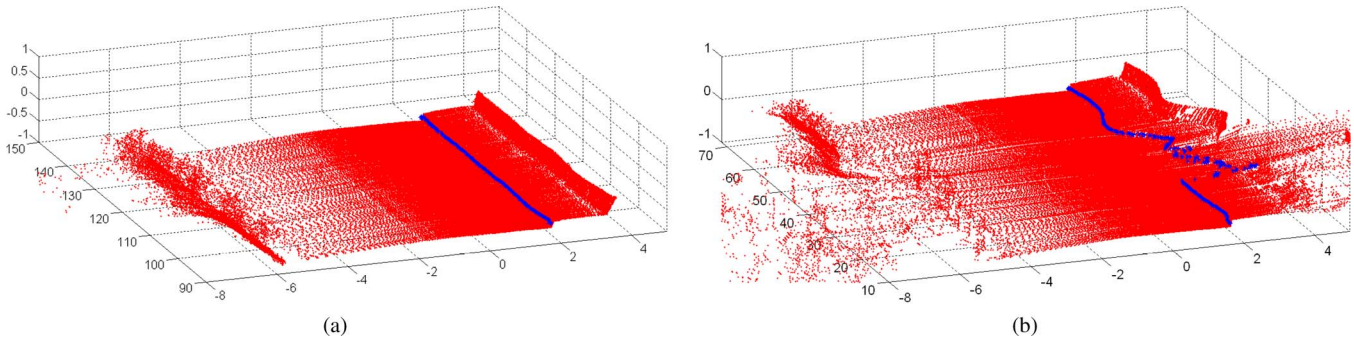

Fig. 9. (a) Result of curb detection for a straight road with a roadside curb. (b) Result of curb detection for a road with an intersection.

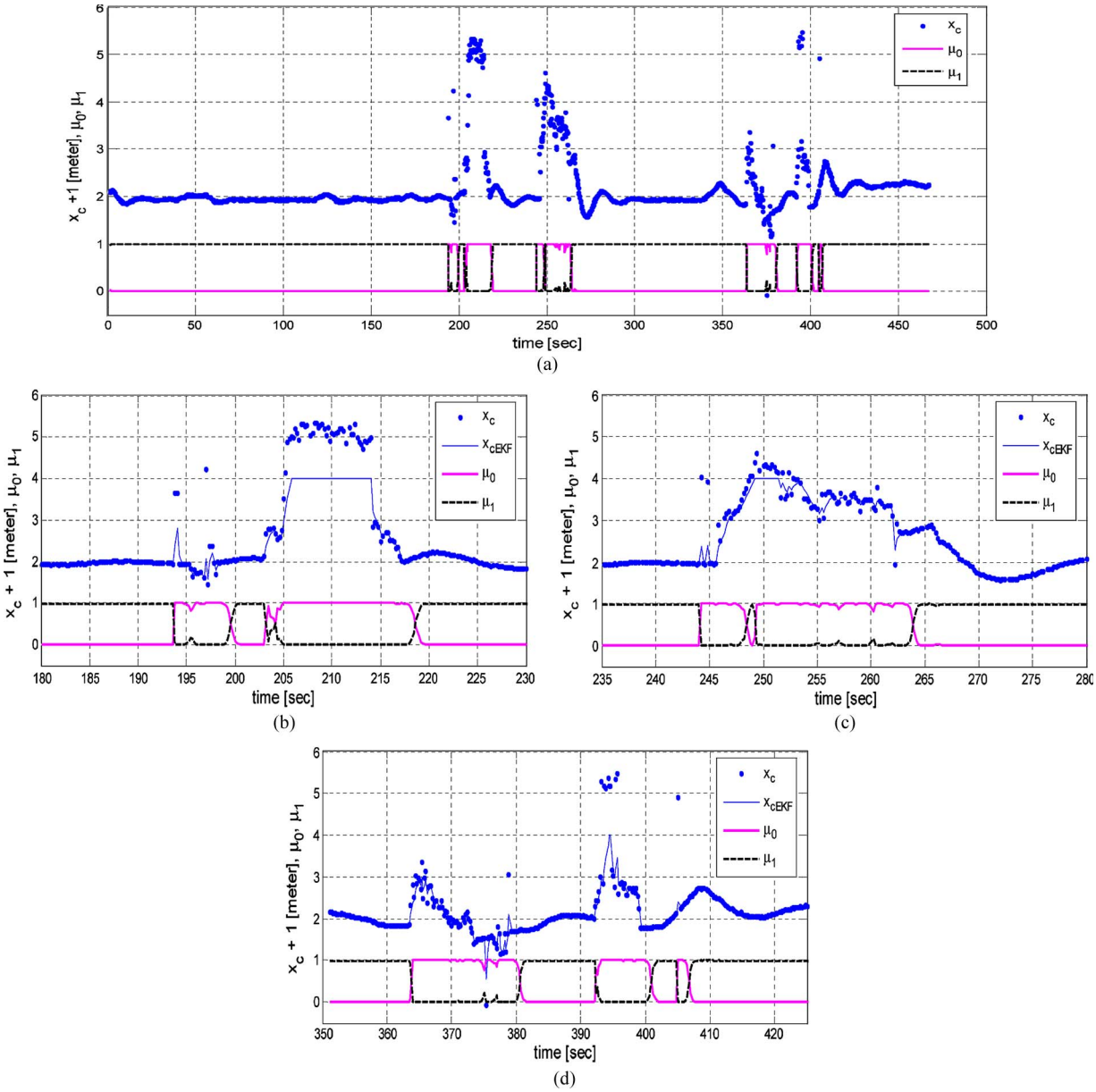

Fig. 10. (a) Experimental result of the curb detection x_c, the Kalman filter estimation x_{cEKF}, and model probabilities μ_0 and μ_1 from the IMM algorithm. (b)–(d) Enlarged pictures when the robot is crossing the intersection.

localize the robot's position on the planned route, although the actual control algorithm uses the relative curb position for feedback. Route planning to the robot's destination is based on the robot's current global position estimate and the route map.

The parameters required for the IMM-based decision-making algorithm were set as provided in Table I, where π_{ij} represents the transition probability between two models. μ_{high} represents the probabilistic threshold to declare that a curb is present,

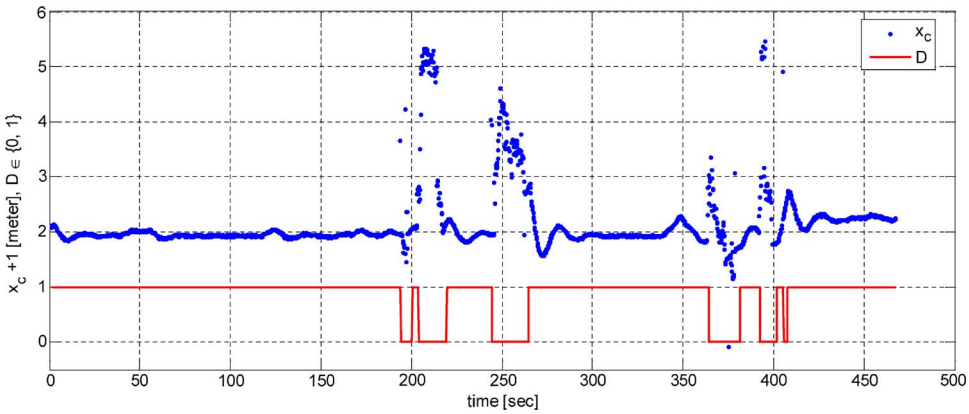

Fig. 11. Result of decision-making variable $D(k)$ on the existence of curb during the overall experiment.

and μ_{low} represents the threshold to declare that a curb is not present. S_0 and S_1 represent the measurement noise covariance matrices for the models explained in Section III-B. In order to eliminate false decisions, the actual switching of the control mode occurs after the decision variable $D(k)$ changes from the current status for several consecutive steps. The forward velocity of the mobile robot is kept at approximately 1 m/s. The lidar measurements scan the road surface at 5 Hz, 2 m ahead of the robot.

Fig. 9(a) shows the set of lidar measurements and curb detection algorithm outputs for a curbed road. Fig. 9(b) shows the experimental results for a road where the curb is discontinued for a while. The proposed curb detection algorithm is accurate: The curb point position error is less than 2–5 cm on average. However, when the curb is discontinued, the curb point trajectory has large fluctuations because of a large resolution error as shown in Fig. 4.

Fig. 10(a) shows the model probability calculated from the IMM algorithm and the curb position estimation. In the plot, $x_c + 1$ is plotted instead of x_c to avoid overlapping between the probability plot and the measurement plot. From the x_c measurement plot, it is noted that the robot successfully maintains a distance of 1 m from the curb, even though there were several intersections and speed bumps. The robot deviates from the desired position slightly when the robot is controlled by dead-reckoning control for a while. As soon as the robot detects the curb from the lidar scan, it quickly switches to the curb-following control mode and converges to the desired distance from the curb. Fig. 10(b) also shows that a saturation limit is set on the Kalman filter estimate to avoid unnecessary deviation of the estimate for the case of no curb. The solid and dotted lines in the figure show μ_0 and μ_1, respectively. μ_0 represents the probability that there is no curb in the lidar's field of view, and μ_1 represents the probability that there is a curb. Fig. 10(b)–(d) shows enlarged plots of Fig. 10(a) when the robot passes intersections. As shown in Fig. 10(b), μ_0 increases sharply around 193 s as the measurement shows a large deviation from the predicted position of the curb. This sudden jump in the measurement originates from the irregularity of the road's surface due to the speed bump on the road. The algorithm determines that it is unlikely that the measurement originates from a real curb. As shown in Fig. 11, the decision variable is switched from one to zero after μ_0 is above the probabilistic threshold of 0.9. After the robot passes the speed bump, μ_1 increases almost to unity. When the robot reaches the intersection immediately after the speed bump, the probability μ_0 increases again, and the intersection is detected by the algorithm.

Fig. 10(c) shows the robot detecting the second intersection as the probability increases at around 243 s. Fig. 10(d) shows the robot detecting the third and fourth intersections at around 365 and 392 s, respectively. At around 405 s, there is one false detection due to one measurement jump.

Fig. 11 shows the decision-making result generated from the model probability shown in Fig. 10. The red solid line represents the decision variable $D(k)$. As the decision variable switched, the mobile robot switched its controller from the curb-following control to its dead-reckoning control. After the mobile robot successfully crosses the intersection and the curb continues, the robot switches to curb-following control as the probability μ_1 gradually increases up to the designated threshold.

V. Conclusion

We have proposed a probabilistic decision-making algorithm that uses the IMM method for autonomous mobile robot navigation. An example of the successful experimental results was presented and analyzed in detail in Section IV. The proposed method was verified in many closed-loop experiments in which the control mode was switched by the algorithm's decision results. Using the proposed algorithm, the robot successfully navigated on a road with several intersections. The decision-making algorithm worked robustly against environmental changes. Performance was enhanced by enabling the robot to be reactive to changes in the information source particularly when the GPS was unreliable. In particular, the dead-reckoning distance could be significantly decreased, which could cause an accumulation of error if the actual switching is determined by an unreliable global position estimate of the robot. Based on the proposed decision-making method, a more reliable navigation strategy can be developed using environmental feature information extracted from multiple sensors such as vision and infrared in addition to lidar. One possible future extension can be the use of the whole lidar scan for the multiple Kalman filter updates.

REFERENCES

[1] J. Vandorpe, H. Van Brussel, and H. Xu, "Lias: A reflexive navigation architecture for an intelligent mobile robot system," *IEEE Trans. Ind. Electron.*, vol. 43, no. 3, pp. 432–440, Jun. 1996.

[2] M. Kam, X. Zhu, and P. Kalata, "Sensor fusion for mobile robot navigation," *Proc. IEEE*, vol. 85, no. 1, pp. 108–119, Jan. 1997.

[3] S. Panzieri, F. Pascucci, and G. Ulivi, "An outdoor navigation system using GPS and inertial platform," *IEEE/ASME Trans. Mech.*, vol. 7, no. 2, pp. 134–142, Jun. 2002.

[4] T. Sasaki, D. Brščić, and H. Hashimoto, "Human-observation-based extraction of path patterns for mobile robot navigation," *IEEE Trans. Ind. Electron.*, vol. 57, no. 4, pp. 1401–1410, Apr. 2010.

[5] U. Larsson, J. Forsberg, and Å. Wernersson, "Mobile robot localization: Integrating measurements from a time-of-flight laser," *IEEE Trans. Ind. Electron.*, vol. 43, no. 3, pp. 422–431, Jun. 1996.

[6] W. Chung, S. Kim, M. Choi, J. Choi, H. Kim, C. Bae Moon, and J.-B. Song, "Safe navigation of a mobile robot considering visibility of environment," *IEEE Trans. Ind. Electron.*, vol. 56, no. 10, pp. 3941–3949, Oct. 2009.

[7] J. C. Mccall and M. M. Trivedi, "Video-based lane estimation and tracking for driver assistance: Survey, system and evaluation," *IEEE Trans. Intell. Transp. Syst.*, vol. 7, no. 1, pp. 20–37, Mar. 2006.

[8] T.-H. S. Li, Y.-C. Yeh, J.-D. Wu, M.-Y. Hsiao, and C.-Y. Chen, "Multifunctional intelligent autonomous parking controllers for carlike mobile robots," *IEEE Trans. Ind. Electron.*, vol. 57, no. 5, pp. 1687–1700, May 2010.

[9] Y. Morales, E. Takeuchi, A. Carballo, W. Tokunaga, H. Kuniyoshi, A. Aburadani, A. Hirosawa, Y. Nagasaka, Y. Suzuki, and T. Tsubouchi, "1 km autonomous robot navigation on outdoor pedestrian paths 'Running the Tsukuba Challenge 2007'," in *IEEE Int. Conf. Intell. Robots Syst.*, Sep. 2008, pp. 219–225.

[10] W. Wijesoma, K. Kodagoda, and A. P. Balasuriya, "Road-boundary detection and tracking using ladar sensing," *IEEE Trans. Robot. Autom.*, vol. 20, no. 3, pp. 456–464, Jun. 2004.

[11] S.-H. Kim, C.-W. Roh, S.-C. Kang, and M.-Y. Park, "Outdoor navigation of a mobile robot using differential gps and curb detection," in *Proc. IEEE Int. Conf. Robot. Autom.*, 2007, pp. 3414–3419.

[12] K. R. S. Kodagoda, W. S. Wijesoma, and A. P. Balasuriya, "Cute: Curb tracking and estimation," *IEEE Trans. Control Syst. Technol.*, vol. 14, no. 5, pp. 951–957, Sep. 2006.

[13] K. Peterson, J. Ziglar, and P. E. Rybski, "Fast feature detection and stochastic parameter estimation of road shape using multiple lidar," in *Proc. IEEE/RSJ Int. Conf. Intell. Robots Syst.*, 2008, pp. 612–619.

[14] D. S. Caveney and J. K. Hedrick, "Multiple target tracking in the adaptive cruise control environment using multiple models and probabilistic data association," in *Proc. ASME IMECE*, 2001, pp. 1–50.

[15] N. Kaempchen, K. Weiss, M. Schaefer, and K. C. J. Dietmayer, "IMM object tracking for high dynamic driving maneuvers," in *Proc. IEEE Intell. Veh. Symp.*, Jun. 2004, pp. 825–830.

[16] C.-C. Wang, C. Thorpe, and A. Suppe, "Ladar-based detection and tracking of moving objects from a ground vehicle at high speeds," in *Proc. IEEE Intelligent Vehicles Symposium*, Jun. 2003, pp. 416–421.

[17] Y. Zhang and X. R. Li, "Detection and diagnosis of sensor and actuator failures using imm estimator," *IEEE Trans. Aerosp. Electron. Syst.*, vol. 34, no. 4, pp. 1293–1313, Oct. 1998.

[18] C. Rago, R. Prasanth, R. K. Mehra, and R. Fortenbaugh, "Failure detection and identification and fault tolerant control using the IMM-KF with application to the eagle-eye uav," in *Proc. IEEE Conf. Decision Control*, Dec. 1998, pp. 4208–4213.

[19] M. Efe and D. P. Atherton, "The IMM approach to the fault detection problem," in *Proc. IFAC Symp. Syst. Identification*, Jul. 1997, pp. 625–630.

[20] Y. Kang, D. S. Caveney, and J. K. Hedrick, "Performance analysis of an IMM-based obstacle detection algorithm," in *Proc. ASME Int. Mech. Eng. Conf. RD&D Expo.*, Nov. 2004, pp. 635–644.

[21] Y. Kang, D. S. Caveney, and K. Hedrick, "Real-time obstacle map building with target tracking," *J. Aerosp. Comput. Inf. Commun.*, vol. 5, pp. 120–134, May 2008.

[22] Y. Bar-Shalom and T. E. Fortmann, *Tracking and Data Association*. Boston, MA: Academic, 1988.

[23] Y. Bar-Shalom and X. R. Li, *Multitarget-Multisensor Tracking: Principles and Techniques*. Storrs, CT: YBS, 1995.

[24] E. Frew, T. McGee, Z. Kim, X. Xiao, S. Jackson, M. Morimoto, S. Rathinam, J. Padial, and R. Sengupta, "Vision-based road following using a small autonomous aircraft," in *Proc. IEEE Aerosp. Conf.*, 2004, pp. 3006–3015.

[25] Y. Kanayama, Y. Kimura, F. Miyazaki, and T. Noguchi, "A stable tracking control method for an autonomous mobile robot," in *Proc. IEEE Int. Conf. Robot. Autom.*, 1990, pp. 384–389.

Yeonsik Kang received the Ph.D. degree in mechanical engineering from the University of California (UC), Berkeley, in 2006.

He was a Postdoctoral Researcher with the Center for Collaborative Control of Unmanned Vehicles, UC Berkeley, in 2006–2007. He was a Senior Researcher Scientist with the Center for Cognitive Robotics Research, Korea Institute of Science and Technology, Seoul, Korea, in 2007–2010. Since 2010, he has been a Professor with the Department of Automotive Engineering, Kookmin University, Seoul. His research interests include navigation, nonlinear control, and target tracking.

Chiwon Roh received the B.S. degree, the M.S. degree in control instrument engineering, and the Ph.D. degree in electrical engineering from Ajou University, Suwon, Korea, in 1995, 1997, and 2007, respectively.

From 1997 to 1999, he was with LG Industrial Systems as a Research Engineer and with the Korea Institute of Science and Technology, Seoul, Korea, as a Postdoctoral Researcher from 2007 to 2009. He is currently with Yujin Robot Company, Ltd., Seoul. His research areas are autonomous mobile robot navigation and intelligent service robot system.

Seung-Beum Suh received the B.S. degree in mechanical engineering from the University of California, San Diego, in 2006 and the M.S. degree in mechanical engineering from the University of Michigan, Ann Arbor, in 2007.

Since 2007, he has been a Research Scientist with the Korea Institute of Science and Technology, Seoul, Korea. His research interests include mobile robot navigation and image processing.

Bongsob Song received the B.S. degree in mechanical engineering from Hanyang University, Seoul, Korea, in 1996 and the M.S. and Ph.D. degrees in mechanical engineering from the University of California (UC), Berkeley, in 1999 and 2002, respectively.

He was a Research Engineer with the California Partners for Advanced Transit and Highways Program, UC Berkeley, until 2003. He is currently an Associate Professor with the Department of Mechanical Engineering, Ajou University, Suwon, Korea. His research interests include sensor fusion, convex optimization, and nonlinear and robust control with applications to intelligent vehicles.